Impact of Atmospheric Icing on UAV Aerodynamic Performance

Richard Hann*, Andreas Wenz*, Kristoffer Gryte*, Tor Arne Johansen*
*Centre for Autonomous Marine Operations and Systems
Department of Engineering Cybernetics
Norwegian University of Science and Technology, Trondheim, Norway

Abstract—This paper presents a first assessment on the impact of atmospheric icing on the aerodynamic performance of fixed-wing UAVs. Numerical simulations were performed in order to evaluate the impact on lift and drag on a 2D airfoil for UAVs. The results show clear evidence that icing increases drag while decreasing lift and the maximum angle of attack. All these effects have negative impact on the maneuverability, stall behavior, range and general operational capabilities of UAVs. Additionally, these results were used in a flight simulator in order to allow the simulation of UAV flights in icing conditions and to study the impact of icing on energy consumption and autopilot responses. Results from the flight simulator show higher angles of attack and higher energy consumption when flying in icing conditions. This flight simulator provides a testbed for further research into in-flight ice detection for fixed-wing UAVs.

I. INTRODUCTION

In recent years, there has been a strong development and an increased utilization of unmanned aerial vehicles (UAVs). These automated drones are suitable for a wide range of applications and are used in many different industries or science areas today. Fixed-wing UAVs are well suited for remote sensing operations in isolated and harsh areas, such as the Arctic. However, cold climate conditions impose special challenges for UAV operations. This is a topic that has only recently shifted into the focus of research.

The main problem for fixed-wing UAVs in cold climate conditions is atmospheric icing [10]. This type of icing occurs when super-cooled cloud droplets collide with the leading-edge of the vehicle and form ice. This ice is considered to cause a significant reduction in the aerodynamic performance. Icing has been attributed as the main reason for UAV losses in cold climate regions.

Atmospheric icing is not an issue only affecting UAVs. It is also relevant for general aviation, wind turbines and building structures (e.g. power lines or masts). As such, there has already been significant research performed on the topic, with the main focus being on aircraft icing. Transferring results from (commercial or military) aircrafts to UAVs is not a trivial task for a number of reasons. The main one being the difference in the Reynolds (Re) number regime between the two applications. Aircrafts are typically operating at relatively high Reynolds numbers $Re = [1..10 \times 10^6]$. Due to their smaller size and generally lower velocities, UAVs operate in the low-Reynolds number regime $Re = [1..10 \times 10^5]$.

The difference of approximately one order of magnitude in the Reynolds number has a significant impact on the flow characteristics. At low Reynolds numbers, the viscous forces are dominating over the inertial forces, which means that viscous boundary layer effects are more significant. For example, the transition point between laminar and turbulent flow occurs later (i.e. more downstream) for low Reynolds numbers. In addition, laminar separation almost exclusively occurs in the low Reynolds number regime. For this reason it is necessary to study the impact of atmospheric icing on UAVs specifically.

Recently there have been research efforts to detect icing in flight [5], [13], [14], [16]. Test flights with real UAVs in icing conditions are risky and it is challenging to acquire reliable baseline data of the aerodynamic coefficients in icing. Therefore there is a need to generate datasets using flight simulators that can simulate the behavior of an UAV in icing conditions to be able to test and develop new icing detection algorithms.

This paper makes an assessment of the impact of icing on the aerodynamic performance by using simulation tools and generic meteorological icing cases. The resulting lift, drag and momentum coefficients are then implemented in an existing UAV simulator and implications of icing on the autopilot reaction are studied.

II. METHOD

For low Reynolds numbers with free transition, computational fluid dynamics (CFD) is typically unable to predict lift and drag accurately. This is due to the occurrence of laminar separation effects (e.g. laminar bubbles) which cannot be captured fully with common CFD methods [3]. In order to mitigate this problem, the calculations were performed fully turbulent. This assumption is considered to be acceptable because the ice accretion at the leading-edge is typically resulting in surface roughness heights large enough to trigger laminar-turbulent transition.

A. Numerical Tools

Several simulation tools have been utilized for this study. For the generation of 2D ice shapes, the LEWICE code (version 3.2.2) has been applied [17]. LEWICE is a widely used 2D ice accretion tool that has been developed for aerospace applications and which has been validated over
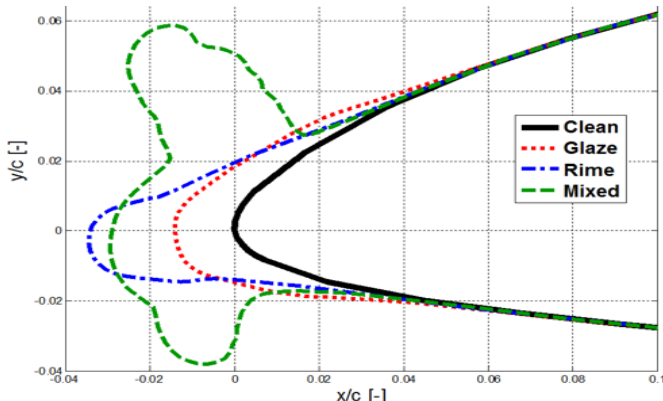
Fig. 1: Icing test cases geometry

TABLE I: Icing Test Cases

Parameter	Icing Type		
	Glaze	*Mixed*	*Rime*
v_{icing}	$25 m/s$	$40 m/s$	$25 m/s$
t_{icing}	40 min	40 min	40 min
c	$0.3m$	$0.3m$	$0.3m$
α_{icing}	$0°$	$0°$	$0°$
MVD	$30 \mu m$	$20 \mu m$	$20 \mu m$
LWC	$0.34 g/m^3$	$0.55 g/m^3$	$0.44 g/m^3$
T_∞	$-2°C$	$-4°C$	$-10°C$
k_s	$0.6mm$	$1mm$	$1mm$

a large range of parameters [18]. However, LEWICE is limited to Reynolds numbers above 2.3×10^6 which falls out of the range for most UAV applications. However, there is indications that the simulation methods used are also applicable for lower Reynolds numbers, as long as there are no major low Reynolds effects present [9] [7]. A strict proof of this is however still missing and should be investigated in the future.

The flow field around the iced geometries was solved with FENSAP, a state-of-the-art Reynolds-Averaged Navier-Stokes CFD solver [6]. The solver is part of the software package FENSAP-ICE which is a 3D icing simulation tool. In this study however, for the sake of simplicity, LEWICE was used for the ice generation and FENSAP only as a steady-state flow field solver. The turbulence model has been chosen as Spalart-Allmaras since it performs well for turbulent flows with negative pressure gradients [15]. Furthermore a streamline upwind artificial viscosity is used.

B. Geometry and Test Cases

In order to assess the impact of icing on the aerodynamic performance of UAVs, icing was simulated on a 2D airfoil. The NREL S826 airfoil was selected due to the availability of experimental data to validate the simulation results [4]. The S826 airfoil was developed for $20 - 40m$ diameter horizontal-axis wind turbines with variable-pitch control. The main characteristics of the airfoil are a high lift-to-drag ratio, docile stall characteristics and insensitivity to transition [12]. This makes them relevant for UAV purposes (e.g. for long-endurance designs), although the design Reynolds number of 1.5×10^6 is slightly higher than most UAV applications.

Icing cases are generally defined by the following parameters: free stream icing velocity v_{icing}, duration of icing t_{icing}, airfoil chord length c, angle of attack α_{icing}, liquid water content LWC, median volume diameter MVD and ambient temperature T_∞ [17]. For this study, a large number of combinations of these parameters have been simulated with LEWICE in order to find representative ice shapes for different icing cases. Based on the geometrical characteristics of the ice accretion such as location, extent, size, curvature,

three ice shapes have been selected, Figure 1. In accordance with certification regulations of aircraft icing, an empirical correlation for droplet size and water content applicable for stratus clouds has been used [8]. The icing cases are mainly distinguished by the temperature at which they form and are summarized in table I.

Glaze ice is an ice type that forms at temperatures very close to freezing conditions. It is dominated by a low mass fraction of particles that freeze on impact. The majority of droplets form a liquid water film on the surface of the airfoil which will either freeze or evaporate. Due to aerodynamic friction, the liquid film will be flowing downstream as so-called runback. Glaze typically appears as transparent ice with a typically smooth surface. At very low temperatures, all droplets freeze on impact and form rime ice. Due to entrapped air between the frozen droplets, rime appears as white and displays rugged, rough surface. Rime is one of the most commonly encountered ice forms in aviation. Mixed icing is an ice type that is formed in the temperature regime between rime and glaze. Therefore, it is characterized by a balanced ratio between instantaneous freezing and surface freezing. Due to this characteristic, the mixed ice builds up ice horns at an approximately $45°$ angle.

The surface roughness k_s for each icing case was approximated using empirical correlations [11]. Generally, surface roughness is mainly driven by temperature and velocity, but also by droplet size. In cases with significant amount of instantaneous freezing (rime and mixed), the roughness will be larger than for cases with surface freezing (glaze). It should be noted that the selected ice shapes may not be entirely representative for each icing type as ice shapes vary extensively over the parameters stated above. However, they serve well to give an overview of the main mechanisms and impacts.

In this work, the complexity of the problem was reduced by only performing 2D simulations. Quantitative transferal of 2D simulations to 3D and to real-life flight characteristics is limited. However, it is considered that that the results allow for a qualitative assessment of the icing impact.

III. SIMULATION RESULTS

To evaluate the aerodynamic performance impact of icing, three key dimensionless characteristics are considered. The

lift coefficient $C_{L_\alpha,airfoil}$ represents the uplift force generated by the airfoil, the drag coefficient $C_{D_\alpha,airfoil}$ relates to the resisting force of the airfoil and the moment coefficient $C_{M_\alpha,airfoil}$ to the resulting airfoil moment [1]. All coefficients are related quadratic to the velocity and linearly to air density and chord length. Experimental validation results
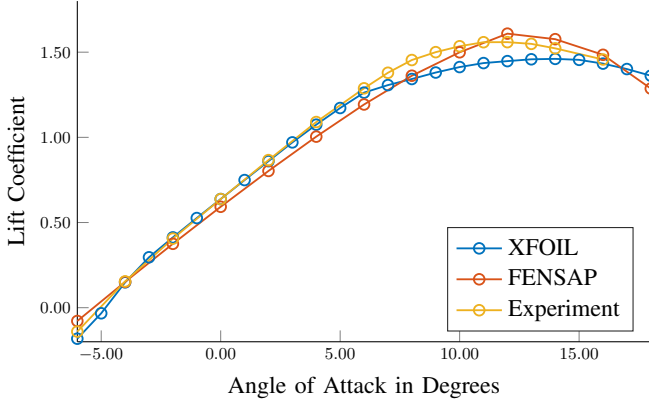

Fig. 2: Experimental and simulation lift coefficient curves for the clean NREL S826 airfoil at $Re = 2 \times 10^5$

to verify the FENSAP simulations have been generated in a wind tunnel study using 3D printed artificial ice shapes on the NREL S826 airfoil [4]. An example for this is depicted in Figure 2 for the clean case. In general, the experimental data shows good fit with both simulation results in the linear section of the lift curve. The FENSAP results show a slight deviation of the gradient, which can be attributed to the simulations being run fully-turbulent and thus not catching any laminar effects. For the same reasons FENSAP may slightly over-predict the maximum lift angle and maximum lift value. In the stall region, XFOIL shows an early onset of the trailing edge stall and a low maximum lift. This is likely to be related to the inaccurate formulation of the turbulent flow behavior inherent to any 2D panel code. The validation results for the drag coefficient as well as icing cases are not shown here, but exhibit the same good fit with similar behavior as for the lift coefficient. In addition, comparisons between numerical and experimental pressure distributions can also be found in the study [4]. All icing cases show a clear negative impact on the aerodynamic performance. The lift curves in Figure 3 are affected in two ways. First, the maximum lift angle is clearly reduced in all cases. A reduction of the maximum lift angle will negatively influence the stall behavior of a UAV. This is particularly relevant when operating at low velocities where high angles of attack are required to generate sufficient lift. The reduction of maximum lift and lift angle may also be a critical issue for UAVs that facilitate for deep-stall landing maneuvers. The second effect is that for the mixed icing case the lift curves are shifted to lower values. This means that to maintain a specific point in the flight envelope, either the angle of attack (AOA) or the velocity of the UAV has to be increased. As stated earlier, increasing the AOA is linked to an elevated risk for stall. The gradient of the lift curves seems not to be affected in a
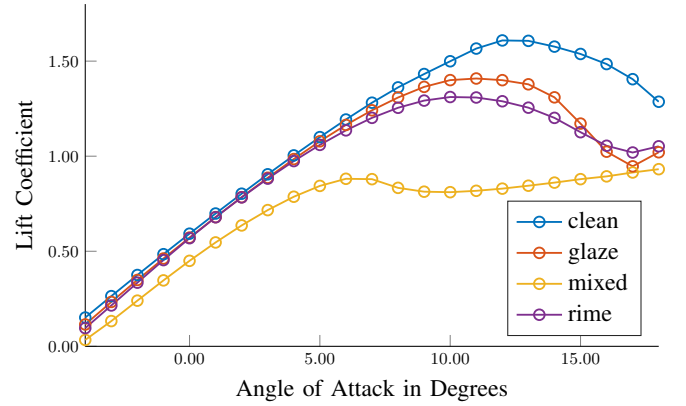

Fig. 3: FENSAP simulation results of the lift coefficient ($C_{L_\alpha,airfoil}$) curves for the clean and iced NREL S826 airfoil at $Re = 2 \times 10^5$

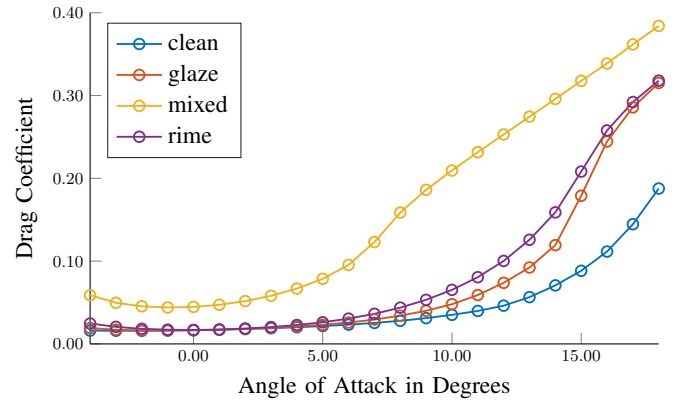significant way for either case. The drag curves in Figure 4

Fig. 4: FENSAP simulation results of the drag coefficient ($C_{D_\alpha,airfoil}$ = curves for the clean and iced NREL S826 airfoil at $Re = 2 \times 10^5$

show that all icing cases increase the aerodynamic resistance compared to the clean case. The increase in drag is larger for high AOAs. This is due to an earlier onset of trailing-edge separation. Again, the drag increase is most severe for the mixed icing case. Therefore the thrust will have to be increased in order to overcome the additional drag force. As thrust generation is linked to fuel consumption, the effective range is decreased by icing. If a UAV does not have sufficient thrust reserves (i.e. the thrust cannot be increased further), it will have to decrease velocity and increase the AOA, which again is linked to an increased risk of stall.

In general, it can be observed that the type of icing has a significant impact on the severity of the degradation of the aerodynamic performance. Rime and glaze ice have apparently weaker effects on lift and drag than mixed ice. In the region of the lift and drag curve with no flow separation ($\alpha = [-4°..8°]$) rime and glaze show very little deviation from the clean case. Only at the more extreme AOAs the decrease of lift and increase in drag becomes substantial. This can be attributed to the relative smooth geometry which

only affects the onset of trailing-edge flow separation at very high/low AOAs.

Rime ice shows a slightly stronger performance degradation than glaze. This can be attributed to the larger ice accretion and larger surfaces roughness of rime compared to the glaze case. Hence for the rime case the friction in the boundary layer will be increased which leads to higher drag and earlier onset of trailing-edge stall.

Mixed ice is showing the strongest impact on lift, maximum lift angle and drag. The mixed ice geometry is the most complex geometry of all cases, with large convex and concave curvatures. In particular, the ice horns will generate turbulent flow separation on the top and the bottom of the leading edge. Separation bubbles cause increased drag and reduced lift [1]. In addition, the turbulence intensity in the boundary layer will be increased by the leading-edge separation, which will lead to an onset of trailing edge separation at lower AOAs compared to clean, rime and glaze ice.
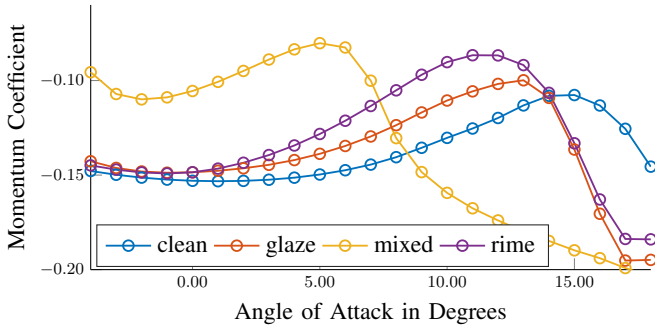

Fig. 5: FENSAP simulation results of the pitch moment coefficient ($C_{M_\alpha,airfoil}$) curves for the clean and iced NREL S826 airfoil at $Re = 2 \times 10^5$

Icing is affecting the pressure distribution over the surface and hence also affecting the pitch moment. Similar to the lift and drag, the biggest impact on the moment curves in Figure 5 can be seen for the mixed icing case and in the stall region. The relatively smooth geometries of glaze and rime follow the trends of the clean curve with some offset at higher angles of attack. For mixed icing the curves shows a significantly abnormal behavior which is again related to the occurrence of the leading edge separation bubbles at the ice horn. The mixed icing case is therefore likely to impose signficant challenges for the stability of the aircraft.

IV. FLIGHT SIMULATION

The lift, drag and pitch moment results from the numerical icing simulation discussed in the previous sections, were used to expand an existing UAV simulator with the capability to simulate flights in icing conditions. The design of the flight simulator mainly follows Beard et.al. [2, c. 3,4] and uses a a dynamic and a kinematic model of the aircraft to simulate its behavior. An autopilot was added to control the simulated aircraft's altitude, course and airspeed using successive loop closure with proportional integral derivative

(PID) controllers and a state machine as described in [2, c. 6]. For a more detailed discussion of the UAV modeling, control and simulation we refer to [2].

In this paper we have focused on the influences of icing on the longitudinal aerodynamic forces. The lift and drag forces for the entire aircraft are given by

$$\begin{bmatrix} f_L \\ f_D \end{bmatrix} = \frac{1}{2}\rho S V_a^2 \begin{bmatrix} C_{L_\alpha}(\alpha) + C_{L_q}(\alpha)\frac{c}{2V_a} + C_{L_{\delta_e}}\delta_e \\ C_{D_\alpha}(\alpha) + C_{D_q}(\alpha)\frac{c}{2V_a} + C_{D_{\delta_e}}\delta_e \end{bmatrix} \quad (1)$$

where V_a is the airspeed, ρ is the air density, S is the wing area, c is the chord length, δ_e is the elevator deflection angle, C_{L_α} is the aerodynamic lift coefficient, C_{D_α} is the aerodynamic drag coefficient, C_{L_q} is the pitch rotation lift coefficient, C_{D_q} is the pitch rotation drag coefficient, $C_{L_{\delta_e}}$ is the elevator lift coefficient and $C_{D_{\delta_e}}$ is the elevator drag coefficient. The lift and drag forces can be converted to body forces using

$$\begin{bmatrix} f_x \\ f_z \end{bmatrix} = \begin{bmatrix} \cos(\alpha) & -\sin(\alpha) \\ \sin(\alpha) & \cos(\alpha) \end{bmatrix} \begin{bmatrix} f_L \\ f_D \end{bmatrix} \quad (2)$$

The pitch moment is given by

$$m = \frac{1}{2}\rho S V_a^2 c \left(C_{m_\alpha}(\alpha) + C_{m_q}(\alpha)\frac{c}{2V_a} + C_{m_{\delta_e}}\delta_e \right) \quad (3)$$

where C_{M_α} is the aerodynamic pitch moment coefficient, C_{m_q} is the pitch dampening coefficient and $C_{m_{\delta_e}}$ is the elevator moment coefficient. We will assume that additional to the NREL S826 airfoil the aircraft is also equipped with a horizontal stabilizer which counteracts the moment created by the airfoil so that the aircraft fulfills trim conditions in clean conditions and normal cruise. Therefore the C_{L_α}, C_{D_α} and C_{M_α} are modeled as follows

$$C_{L_\alpha} = C_{L_\alpha,s} + C_{L_\alpha,airfoil} \quad (4)$$
$$C_{D_\alpha} = C_{D_\alpha,s} + C_{D_\alpha,airfoil} \quad (5)$$
$$C_{M_\alpha} = C_{M_\alpha,s} + C_{M_\alpha,airfoil} \quad (6)$$

where the airfoil parameters are given by the respective curves for each icing scenario shown in Figure 3, Figure 4 and Figure 5. Since the numerical simulations only output discrete values, spline interpolation was used to generate continuous curves . The stabilizer coefficients $C_{L_\alpha,s}$ and $C_{M_\alpha,s}$ are chosen to compensate for the lift and moment created by the airfoil at $\alpha = 0$ and $V_a = 20m/s$. Values for the different coefficients can be found in table II. Where M is the mass of the UAV and P_{motor} is the maximum power of the propulsion system. The coefficients in table II are assumed to be not affected by icing.

TABLE II: Coefficients

Parameter	Value	Parameter	Value
V_a	$20m/s$	$C_{L_{\delta_e}}$	0.587
ρ	$1.2250kg/m^3$	$C_{m_{\delta_e}}$	-0.971
S	$0.25m^2$	$C_{D_{\delta_e}}$	0.846
c	0.36	$C_{L_\alpha,s}$	-0.3
C_{L_q}	3.89	$C_{D_\alpha,s}$	0.01
C_{D_q}	0	$C_{M_\alpha,s}$	0.14
M	$4kg$	P_{motor}	$600W$

V. Flight Simulation Results

In this section results from the flight simulator in different icing conditions are shown. The implementation was done in Matalab / Simulink.

A. Flight scenario

The aircraft is flying in a constant horizontal wind of $8m/s$ added by Dryden wind gusts assuming a wind speed of $6m/s$ at $10m$ above ground. The aircraft's autopilot is set to fly at a constant course and a constant airspeed while performing the altitude changes shown in Figure 6. This scenario is simulated
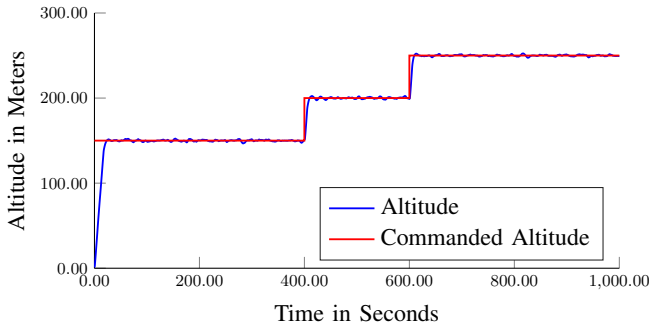
Fig. 6: Commanded and resulting altitude of the UAV

for the three different icing scenarios from table I and the clean case.

B. Angle of Attack

Figure 7 shows the AOA for the entire flight. Notably the AOA does not show a significant difference in the cruise phases between the clean, rime and glaze ice cases. However due to the reduced lift gradient in mixed icing conditions (3) the autopilot adjusts to a higher AOA during cruise, causing the aircraft to stall permanently and thous no stable flight is possible. To circumvent this the airspeed has to be adjusted to a higher value of $22m/s$ in mixed ice. Figure 8 shows the
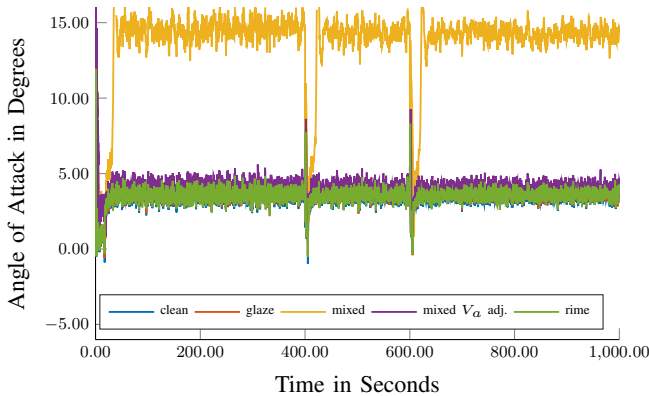

Fig. 7: Angle of Attack for different icing conditions

angle of attack during a climb. The figure clearly shows a significantly increased AOA in the mixed icing cases during climbing compared to the clean case, even with increased airspeed. The difference in AOA is most significant around

$t = 400s$ where the pitch angle is increased and the AOA in the mixed ice case rises above the stall angle (see Figure 3). For the other icing cases AOA is only slightly increased but remains below stall angle. The negative AOA around $t = 405s$ is a result of a negative pitch rotation and compensates for the higher airspeed.
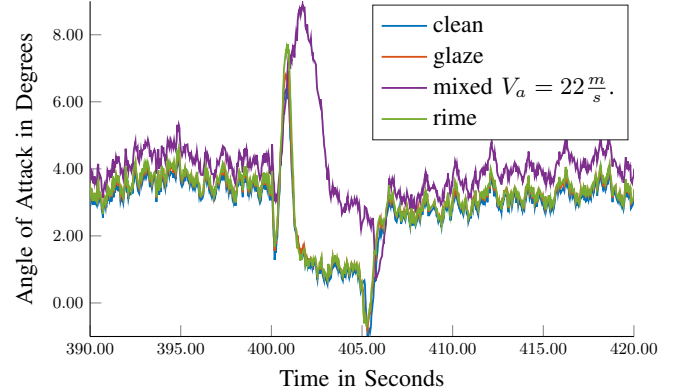

Fig. 8: Angle of Attack during climb for different icing conditions

C. Elevator Deflection

Figure 9 shows the elevator deflection for the entire flight for the different icing scenarios. We see that due to the change in the pitch moment coefficient in the mixed ice case (see Figure 5) the autopilot has to apply a constant elevator deflection in order to keep the aircraft level. Note that in the clean case a small negative deflection is necessary to achieve trim conditions. For the glaze and rime icing scenarios this moment is compensated for by the change in pitch moment coefficient, decreasing the need for elevator deflections.
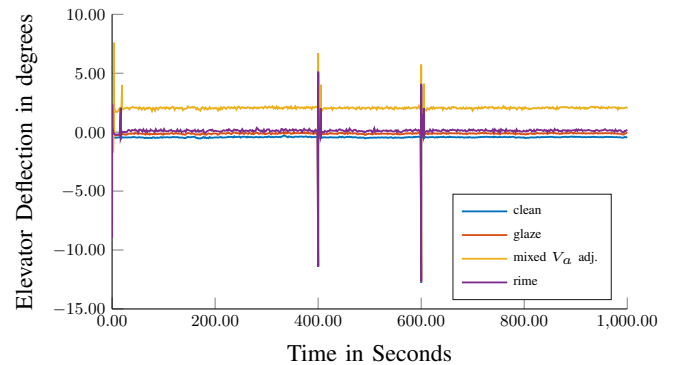

Fig. 9: Elevator Deflection

D. Airspeed

During climbs the autopilot does not hold the airspeed but applies full thrust in order to facilitate the altitude changes more quickly. This leads to deviations from the desired airspeed. Figure 10 shows an example of the airspeed change during an altitude change for the different icing scenarios. The lower airspeed during climb in the mixed icing case is
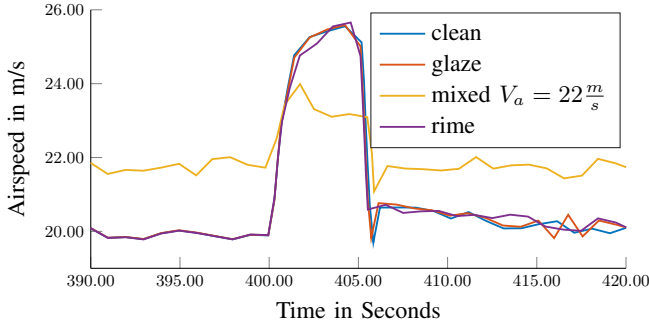
Fig. 10: Airspeed during climb for different icing conditions

caused by the increased drag coefficient and angle of attack. Maximum thrust is applied in these climb phases. This results in a decreased climbing performance in these conditions.

E. Energy Consumption

Table III shows the cumulative energy consumption during flight for the four different scenarios. We see again that

TABLE III: Energy Consumption

Clean	Glaze	Mixed	Mixed $V_a = 22\frac{m}{s}$	Rime
$116Wh$	$115Wh$	$153Wh$	$138Wh$	$116Wh$

the mixed ice case deviates significantly from the other scenarios, both with and without adjusted airspeed. The increased energy consumption is a result of the increased angle of attack and the increased airspeed, which is needed to achieve the required lift force. This means that the drag and thus the energy consumption is not solely increased by the larger parasite drag but also by the suboptimal operation point, leading to a significantly diminished range.

VI. CONCLUSION

In summary, the simulation results have shown a very clear and distinct impact of icing on the aerodynamic performance of a 2D airfoil. Generally, it can be observed that lift and the maximum lift angle are decreased and drag is increased substantially. The geometry of the ice shape has a significant effect on the degree of performance degradation. When separation is present at the leading-edge, the negative impact will be amplified. Hence it can be concluded that icing conditions that lead to the accretion of pronounced ice horns are most intrusive on the airfoil performance. Since icing is driven mostly by temperature it may be concluded that icing at very low temperatures (rime) and at very close to freezing conditions (glaze) are less dangerous to a UAV than intermediate low temperatures (mixed).

Further work should focus on investigating the impact of icing on different kinds of airfoils and over a larger range of atmospheric and operational parameters. In addition, more validation work needs to be performed to build trust towards the simulation results. There are currently ongoing wind tunnel experiments with artificial ice shapes that will provide validation data in the future.

Furthermore we have shown how to implement these results into an existing flight simulator. The simulation results show the reaction of a standard autopilot to the performance and stability degradation in icing conditions and the impact on the energy consumption. These results will be used in the future in order to design novel ice detection methods for UAVs prior to test flights.

VII. ACKNOWLEDGMENTS

REFERENCES

[1] Jd Anderson Jr. *Fundamentals of Aerodynamics*, volume Third Edit. McGraw-Hill, 2001.
[2] Randal W. Beard and Timothy W. McLain. *Small Unmanned Aircraft: Theory and Practice*. Princeton University Press, 2012.
[3] J. Blazek. *Computational fluid dynamics : principles and applications*. Elsevier, 2005.
[4] L. Brandrud and J. Kroegenes. *Aerodynamic Performance of the NREL S826 Airfoil in Icing Conditions*. Master thesis, Norwegian University of Science and Technology (NTNU), 2017.
[5] Andrea Cristofaro, Tor Arne Johansen, and Pedro Aguiar. Icing Detection and Identification for Unmanned Aerial Vehicles : Multiple Model Adaptive Estimation. In *Eur. Control Conf.*, 2015.
[6] W G Habashi, M Aubé, G Baruzzi, F Morency, P Tran, and J C Narramore. FENSAP-ICE: A Fully-3D In-Flight Icing Simulation System for Aircraft, Rotorcraft and UAVs. In *24th Int. Congr. Aeronaut. Sci.*, 2004.
[7] R. Hann, S. Neumann, A. Miller, and J. Dillingh. Thermal analysis of a heated rotor blade for wind turbines. In *Winterwind*, 2012.
[8] Richard K Jeck. Icing Design Envelopes (14 CFR Parts 25 and 29 , Appendix C) Converted to a Distance-Based Format. Technical Report April, Federal Aviation Administration, 2002.
[9] Frank T. Lynch and Abdollah Khodadoust. Effects of ice accretions on aircraft aerodynamics, 2001.
[10] R. A. Siquig. Impact of Icing on Unmanned Aerial Vehicle (UAV) Operations. Technical report, Naval Environmental Prediction Research Facility, 1990.
[11] Jaiwon Shin and Thomas H Bond. Experimental and Computational Ice Shapes and Resulting Drag Increase for a NACA 0012 Airfoil NASA Experimental and Computational Ice Shapes and Resulting Drag Increase for a NACA 0012 Airfoil. In *5th Symp. Numer. Phys. Asp. Aerodyn. Flows*, Long Beach, California, 1992.
[12] Dm Somers. The S825 and S826 Airfoils. Technical Report January, National Renewable Energy Laboratory, 2005.
[13] Kim Lynge Sørensen, Mogens Blanke, and Tor Arne Johansen. Diagnosis of Wing Icing Through Lift and Drag Coefficient Change Detection for Small Unmanned Aircraft. In *IFAC Safeprocess'15*, Paris, 2015.
[14] Kim Lynge Sørensen and Tor Arne Johansen. Flight Test Results for Autonomous Icing Protection Solution for Small Unmanned Aircraft. In *Int. Conf. Unmanned Aircr. Syst.*, Miami, 2017.
[15] P. Spalart and S. Allmaras. A one-equation turbulence model for aerodynamic flows. In *30th Aerosp. Sci. Meet. Exhib.*, 1992.
[16] Andreas Wenz and Tor Arne Johansen. Icing detection for small fixed wing UAVs using inflight aerodynamic coefficient estimation. In *Multiconference Syst. Control*, Buenos Aires, Argentina, 2016.
[17] William Wright. User's Manual for LEWICE Version 3.2. Technical report, QSS Group, Inc., Cleveland, Ohio, 2008.
[18] William B Wright and Adam Rutkowski. Validation Results for LEWICE 2.0. Technical Report January, NASA, 1999.